Catalysis Science & Technology

ROYAL SOCIETY OF CHEMISTRY

PAPER

View Article Online
View Journal | View Issue

Cite this: *Catal. Sci. Technol.*, 2021, 11, 6877

Mechanistic insights into carbamate formation from CO_2 and amines: the role of guanidine–CO_2 adducts†

Jere K. Mannisto, [a] Ljiljana Pavlovic, *[b] Tony Tiainen, [a] Martin Nieger,[a] Aleksi Sahari, [a] Kathrin H. Hopmann [b] and Timo Repo *[a]

Received 9th August 2021,
Accepted 2nd September 2021

DOI: 10.1039/d1cy01433a

rsc.li/catalysis

Capture of CO_2 by amines is an attractive synthetic strategy for the formation of carbamates. Such reactions can be mediated by superbases, such as 1,1,3,3-tetramethylguanidine (TMG), with previous implications that zwitterionic superbase–CO_2 adducts are able to actively transfer the carboxylate group to various substrates. Here we report a detailed investigation of zwitterionic TMG–CO_2, including isolation, NMR behavior, reactivity, and mechanistic consequences in carboxylation of aniline-derivatives. Our computational and experimental mechanistic analysis shows that the reversible TMG–CO_2 zwitterion is not a direct carboxylation agent. Instead, CO_2 dissociates from TMG–CO_2 before a concerted carboxylation occurs, where the role of the TMG is to deprotonate the amine as it is attacking a free CO_2. This insight is significant, as it opens a rational way to design new synthesis strategies. As shown here, nucleophiles otherwise inert towards CO_2 can be carboxylated, even without a CO_2 atmosphere, using TMG–CO_2 as a stoichiometric source of CO_2. We also show that natural abundance ^{15}N NMR is sensitive for zwitterion formation, complementing variable-temperature NMR studies.

Introduction

Amines are highly important building blocks in the synthesis of natural products,[1] fine chemicals[2] and pharmaceuticals.[3] A defining characteristic of amines is their strong affinity for various electrophiles, including CO_2. Conventionally, amine-mediated CO_2-capture has been widely used in industrial gas sorption processes.[4] There is an increasing interest in applying amine CO_2-capture for fine chemical synthesis, because CO_2 is non-toxic, cheap and readily available.[5,6] For example, the amine–CO_2 adduct is attractive as a green pathway to *N*-formylation,[7] methylation,[7] and carbamates (Scheme 1).[8–10]

Primary and secondary alkylamines (nitrogen bound to sp^3-hybridized carbon) react rapidly with CO_2 at ambient pressure and temperature. A carbamic acid is the dominant species in polar aprotic solvents (Scheme 2A).[11] The situation is different in non-polar solvents, where two equivalents of amine react with CO_2 to form a carbamate (salt) (Scheme 2B).[11] Here, one amine acts as a Lewis base towards CO_2, while the other one is a Brønsted base. Early reports in the 1990s found the addition of organic superbases (*e.g.* amidines and guanidines) to be critical for certain amine carboxylations.[16,17] The authors proposed the formation of a mixed species of carbamate: the alkylamine acting as a Lewis base (CO_2-acceptor) with the superbase as a Brønsted base (Scheme 2C). In this work, we will refer to the combination of amine and disparate base as a mixed carbamate. The term provides an important distinction to simple carbamate salts, where two equivalents of the same amine are needed for each CO_2 (Scheme 2B).[8,12,13] Alkyl-mixed carbamates are also reported to react with a second equivalent of CO_2, forming a mixed bicarbamate (Scheme 2D).[12,14,15] Clearly, the addition of a superbase markedly increases the reactivity of alkylamines with CO_2.

The reactivity of aromatic amines (nitrogen bound to sp^2-hybridized carbon) with CO_2 is distinct from alkylamines; aromatic amines as such have no or low conversion (*ca.* 1%) to carbamic acids (Scheme 2A) or carbamates (Scheme 2B) at ambient pressure and temperature.[18] Adequate reactivity is

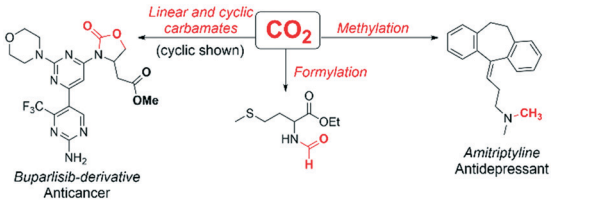

Scheme 1 Selected utilizations of amine–CO_2 adducts.[5–10]

[a] *Department of Chemistry, University of Helsinki, P.O. Box 55, A.I. Virtasen aukio 1, 00014 Helsinki, Finland. E-mail: timo.repo@helsinki.fi*
[b] *Department of Chemistry, UiT The Arctic University of Norway, N-9037 Tromsø, Norway. E-mail: ljiljana.pavlovic@uit.no*

† Electronic supplementary information (ESI) available. CCDC 2044161. For ESI and crystallographic data in CIF or other electronic format see DOI: 10.1039/d1cy01433a

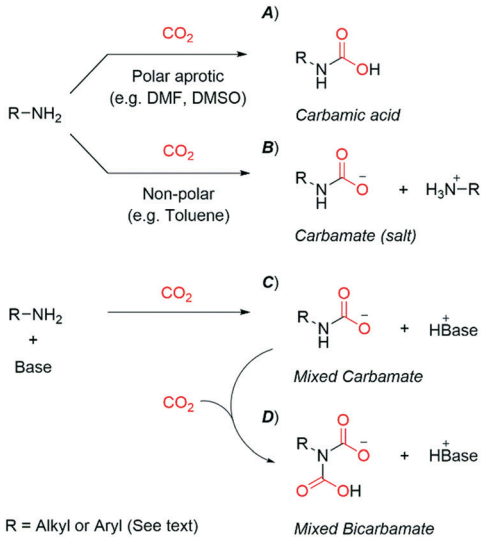

Scheme 2 An overview of reactions involving CO_2-capture by amines, including related nomenclature.[8,11–15]

accessed by the addition of an equivalent of superbase, generating the mixed carbamate (Scheme 2C).[8,12] There is no evidence of mixed bicarbamates of aromatic amines, even in presence of excess superbase.[14] This and the above-mentioned low conversions suggest aromatic amines to be less reactive than alkylamines. Nevertheless, it is clear that superbases significantly increase the reactivity of aromatic amines with CO_2.

Very little is known about the factors that govern mixed carbamate formation from aromatic amines in the presence of superbases. In our previous work, carboxylations were possible using a catalytic amount of superbase, which was regenerated using external base.[8] It has been shown that superbases form adducts with CO_2,[19,20] and it has been proposed that these adducts are a form of "activated CO_2" that mediate the carboxylation step.[8,20–23] However, others have argued that superbase–CO_2 adducts are not active intermediates in carboxylation reactions.[12,24–28] Here, we present a detailed mechanistic study of superbase carboxylation reactivity, using *in situ* NMR studies, isolated reaction intermediates and computational modelling.

Results and discussion

Mixed carbamate mechanistic proposal

To gain insights into mixed carbamate formation with aromatic amines, we first investigated the reaction of 4-nitroaniline (**1**) with CO_2 by NMR. There was no background reaction of **1** under CO_2 (1 atm) in d_6-DMSO. However, in presence of the superbase 1,1,3,3-tetramethylguanidine (TMG), we observed the mixed carbamate **2** in an equilibrium yield of 78% (Scheme 3).

Our results prove that the superbase is essential for mixed carbamate formation from aromatic amines, but they do not give insights into the specific role of the base. We can

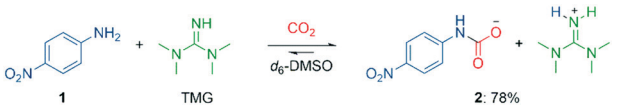

Scheme 3 Carboxylation of 4-nitroaniline (**1**) in presence of TMG and CO_2 in d_6-DMSO. Yield determined by ^{1}H NMR on 0.50 mmol scale.

envision at least three mechanistic possibilities for generation of mixed carbamates from aromatic amines in presence of a superbase (Scheme 4). Path 1 consists of a nucleophilic self-carboxylation. This path is based on recent reports that alkylamines can self-carboxylate with CO_2, forming highly unstable zwitterions, which are deprotonated to carbamate salts.[11] The analogous mechanism with aromatic amines involves two steps (Scheme 4, top): step A consists of a nucleophilic attack of the amine **1** on CO_2, forming zwitterion **3**. Step B consists of a rapid deprotonation by the base, forming the mixed carbamate **2**. Thus in path 1, the superbase acts as a simple Brønsted base after carbamate formation has taken place.

Alternatively, in path 2 (Scheme 4, middle), the superbase may pre-associate with amine **1**, activating it through a concerted event of deprotonation and carboxylation (step C). The concerted mode of activation implies that the nucleophile heteroatom not only must be protic, but also have an available lone pair for interaction with CO_2. In this path, the superbase acts as Brønsted base and as a nucleophile activator. Similar bimolecular Brønsted base-assisted carboxylations have been proposed.[26,29]

In path 3 (Scheme 4, bottom), we assume that CO_2 and the superbase form zwitterionic adduct **4** (step D).[19,20,30] Mixed carbamate formation may then occur through concerted electrophilic carboxylation (step E). At the TS, the zwitterion may be stabilized by hydrogen bonding of the carboxylate and the ammonium protons. Eventually, the zwitterion collapses, simultaneously transferring the carboxylate to **1** and protonating TMG. In this putative

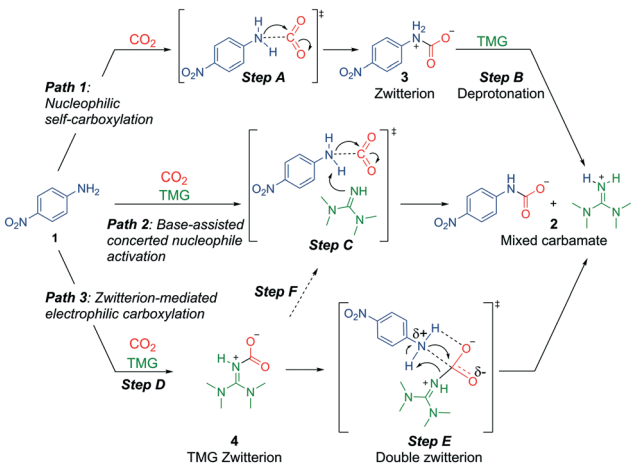

Scheme 4 Three possible mechanistic pathways for mixed carbamate formation from aromatic amines and superbases (in this case 4-nitroaniline and TMG).

mechanism, TMG acts as a transfer-carboxylation agent (as previously proposed in the literature),[20,30] and as a Brønsted base. We note that there also exists the possibility that any formed TMG-zwitterion dissociates prior to carboxylation, which effectively would lead back to path 2 (step F, Scheme 4). The different mechanistic possibilities are investigated in detail below.

The effect of organic base

As part of the mechanistic analysis, we first investigated the effect of various organic bases in the carboxylation of 4-nitroaniline (Table 1). We began by testing alkylamines, which are known to form carbamate salts (Scheme 2B); hence, they may also be able to promote the reaction of 4-nitroaniline and CO_2. Alkylamine DIPA did produce a low amount of mixed carbamate (9%, Table 1, entry 2), in line with previous results (7–17%).[12] Assuming path 1 or 2 are active (Scheme 4), non-nucleophilic bases should produce mixed carbamate *via* simple deprotonation. In path 3 (Scheme 4), the base must first form a CO_2-zwitterion for carboxylation to take place. As DIPA is a secondary amine, it can form a transient CO_2-zwitterion,[11] satisfying the criteria of path 3. Therefore, we wanted to examine a non-nucleophilic base of similar basicity (relevant for path 1 and 2), but unable to form a CO_2-zwitterion, eliminating path 3. In this regard, we used the more bulky DIPEA, which readily scavenges protons, but does not react with most electrophiles,[31] including CO_2.[29,32] No mixed carbamate was observed with DIPEA (Table 1, entry 3). Given that DIPA and DIPEA have very similar basicity, DIPEA should be a strong enough base to deprotonate the nucleophile after N–CO_2 bond formation in path 1, or at the TS of path 2. Since no mixed carbamate was observed, it follows that the formation of a CO_2-zwitterion could be essential (path 3 is active), or that there are other factors than basicity that influence the reaction outcome (such as sterics of the base).[29]

We proceeded to investigate superbases, which are more basic than alkylamines (Table 1, entries 4–8). In general, the yields for these were quite similar; however, bases with a higher Brønsted basicity than TMG did produce more of the mixed carbamate (entries 5, 6 and 8), displaying a linear relationship (R^2 = 0.96, see ESI,† Fig. S1). An exception was TBD, which provided plenty of precipitate and a low amount of mixed carbamate despite high basicity (68%, entry 7). The experiment was repeated at a smaller scale (0.2 mmol) with identical precipitation and yields. Presumably, the low yields are due to unreacted TBD hydrogen-bonding to the mixed carbamate, and the resulting adduct precipitates out.[33] The methylated analogue MTBD was unable to act as a hydrogen bond donor, eliminating competing adduct formation; hence, more carbamate was observed (85%, entry 8, Table 1). Superbase nucleophilicity did not correlate with mixed carbamate yield (R^2 = 0.09, TBD excluded from plot, Fig. S2).[34,35] Overall, the combined superbase results do not provide an unambiguous preference between the mechanistic pathways (Scheme 4).

To obtain more insights into the mechanistic details, we modelled the carboxylation of 4-nitroaniline employing DFT methods (PBE0-D3BJ[IEFPCM] with DMSO as the implicit solvent model, see ESI† section 4). Initially we evaluated the attack of 4-nitroaniline at a free CO_2, corresponding to path 1 (Scheme 4). A TS for this transformation could only be located if an explicit DMSO solvent molecule was added to the molecular model to stabilize the emerging positive charge on nitrogen (Fig. S3†). Although the computed barrier of around 20 kcal mol^{-1} appears surmountable at 298 K (Table 2, entry 1), the resulting protonated carbamate intermediate is highly endergonic, making its formation (and hence path 1) unlikely. Addition of TMG to the model allowed us to compute path 2 (Scheme 4), where the role of the base is to activate the nucleophile.[26] In this model, 4-nitroaniline and TMG form a pre-associated complex, which is slightly more stable than the separated fragments (Fig. S4†), before attack on CO_2 occurs. Pre-association is supported by ^{1}H NMR studies, which show a downfield shift of the –NH_2 of 4-nitroaniline by 0.07 ppm in the presence of TMG under argon. The concerted deprotonation by TMG and attack of the amine on CO_2 (Fig. 1, left) has a barrier of 16.9 kcal mol^{-1} (Table S1,† entry 3), which decreases by 2 kcal mol^{-1}, if an explicit DMSO molecule is included to further stabilize the emerging charges (Table 2, entry 4). The mixed carbamate formation with TMG is computed to be significantly exergonic (Table 2, entry 4), qualitatively supporting the experimentally observed product formation. The computed barrier for the formation of mixed carbamate with TMG is lower by 3.1 kcal mol^{-1} and 3.4 kcal mol^{-1} relative to the computed barriers for DIPA and DIPEA, respectively.

Table 1 The effect of organic base on mixed carbamate formation from 4-nitroaniline

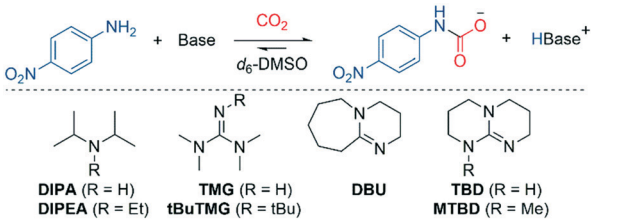

Entry	Base	Yield[a] (%)	pK_a[b] (CH_3CN)
1	4-Nitroaniline	0[c]	6.2 (ref. 36)
2	DIPA	9	18.8 (ref. 37)
3	DIPEA	0[c]	18.6 (ref. 38)
4	TMG	78	23.4 (ref. 39 and 40)
5	*t*BuTMG	92	26.5 (ref. 41)
6	DBU	82	24.3 (ref. 39)
7	TBD	68	26.0 (ref. 39)
8	MTBD	85	25.5 (ref. 39)

[a] Yield of carboxylated 4-nitroaniline determined by ^{1}H NMR on 0.50 mmol scale. [b] pK_a values in CH_3CN are provided, because data in DMSO is not available for all compounds. [c] No carbamic acid nor carbamate salt. Diisopropylamine = DIPA, *N*-ethyldiisopropylamine = DIPEA, 1,8-diazabicyclo[5.4.0]undec-7-ene = DBU, 1,5,7-triazabicyclo[4.4.0]dec-5-ene = TBD, 7-methyl-1,5,7-triazabicyclo[4.4.0]dec-5-ene = MTBD.

Table 2 Computed barriers and Gibbs free energies (kcal mol^{-1}, 298 K)[a] for formation of mixed carbamates from 4-nitroaniline (**1**) using different bases, in the presence of DMSO

Entry	Base	$\Delta G^{\neq b}$ 1 atm [1 M]	ΔG_r 1 atm [1 M]
1	4-Nitroaniline	20.9 [19.0][c]	21.0 [19.1]
2	DIPEA	20.2 [18.3]	2.6 [0.7]
3	DIPA	19.9 [18.0]	1.7 [−0.2]
4	TMG	16.8 [14.9]	−2.2 [−4.1]
5	*t*BuTMG	15.4 [13.5]	−6.2 [−8.1]

[a] PBE0-D3BJ/IEFPCM, see ESI† section 4 for details. Energies are relative to the pre-associated complex 4-nitroaniline-DMSO (entry 1) or 4-nitroaniline-base-DMSO (entries 2–5) and are given as computed (1 atm) and with a standard state correction to 1 M. [b] Barrier for path 2 (Scheme 4). [c] Barrier for path 1 (Scheme 4).

The alternative path 3 involves formation of a TMG–CO_2 zwitterion (Scheme 4). In our calculations, formation of this complex has a low barrier and is slightly endergonic (Fig. 1, right side), indicating that TMG–CO_2 may be present in the reaction mixture in low concentrations. However, a transition state for CO_2 transfer from TMG–CO_2 to 4-nitroaniline could not be located, as the zwitterion always dissociates prior to formation of the aniline–CO_2 bond. From this, we conclude that a TMG–CO_2 zwitterion is unlikely to be an active carboxylation agent and that aniline carboxylation most likely occurs through path 2, where TMG activates the nucleophile through concerted deprotonation. In this scenario, any formed TMG–CO_2 zwitterion would simply be a reversible side product in the reaction mixture.

Calculations on other organic bases (Table 2, entries 2,3,5) show good agreement with the experimental results (Table 1), further supporting that path 2 is the operative mechanism. The computed reaction energy for *t*BuTMG is more exergonic than that for TMG, whereas with DIPEA and DIPA, the carboxylation barrier increases and the reaction is less exergonic. We also performed additional calculations with B3LYP-D3 as an alternative method. The same trend is observed, where the computed barriers and reaction energies with DIPA and DIPEA

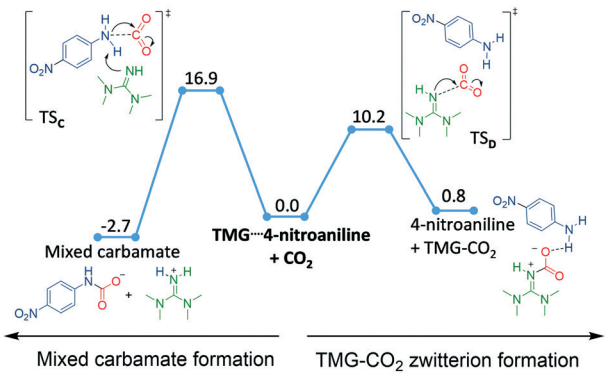

Fig. 1 Computed Gibbs free energies (1 M energies, kcal mol^{-1}, 298 K, PBE0-D3BJ/IEFPCM) and schematic TS structures for carboxylation of 4-NO_2–aniline *via* path 2 (TS_C) compared to formation of the TMG–CO_2 zwitterion (TS_D).

are higher relative to TMG (Tables S1 and S2†). A direct quantitative agreement between the computed reaction energies (Table 2) with the observed reaction yields (Table 1) cannot be expected for the simple computational model used here (which treats the bulk solvent as a homogeneous medium). However, we note that the general trend is reproduced well, indicating that the computational model is able to capture the relative effects that govern the reactivities.

Substituent effects

The effect of aniline substitution was investigated through a Hammett study on the product equilibria of various 4-substituted anilines (Fig. 2). The conditions were similar as in Table 1, employing TMG as a base. Under these conditions, unsubstituted aniline[8] and 4-methoxyaniline converted fully to the mixed carbamate (ESI† section 16). Since electron-rich anilines carboxylated quantitatively, we excluded them from the Hammett study.[42] The Hammett equation is usually used in the context of reaction rates, but the equation also applies to equilibria (eqn (1)), and can be rearranged into a linear form (eqn (2)).[43]

$$\log \frac{K}{K_0} = \sigma\rho \tag{1}$$

$$\log K = \sigma\rho + \log K_0 \tag{2}$$

In mixed carbamate formation, aniline and TMG react in a 1 : 1 manner (eqn (3), R ≠ H).[14] Our experiments were performed with an equimolar amount of the individual aniline and TMG. Therefore, the equilibrium constant K (eqn (4)) could be simplified (eqn (5)). Equilibrium contribution of zwitterion **4** is considered negligible. Next, we defined F as the fraction of mixed carbamate formed in relation to the total amount of aniline (eqn (6)). We were able to measure F conveniently by ^{1}H NMR spectroscopy. Eqn (5) and (6) allowed us to define the equilibrium constant K as a function of F (eqn (7)). Next, by substituting K in eqn (2), we were able to express the Hammett relationship as a function of F (eqn (8)). For derivation details, see ESI† section 5.

In our experiments, mixed carbamate formation was assumed to be in rapid equilibrium, and stable at the time of the measurement by NMR, as confirmed by performing a second NMR experiment 8 or 12 h later with identical results (ESI† section 17). In addition, all measurements were done at the same CO_2 pressure (1 atm), thus we assumed the concentration of CO_2 was constant in all samples.

$$RC_6H_4NH_2 + TMG + CO_2 \rightleftharpoons RC_6H_4NHCO_2^- + TMGH^+ \tag{3}$$

$$K = \frac{[RC_6H_4NHCO_2^-][TMGH^+]}{[RC_6H_4NH_2][TMG][CO_2]} \tag{4}$$

$$K = \frac{[RC_6H_4NHCO_2^-]^2}{[RC_6H_4NH_2]^2[CO_2]} \tag{5}$$

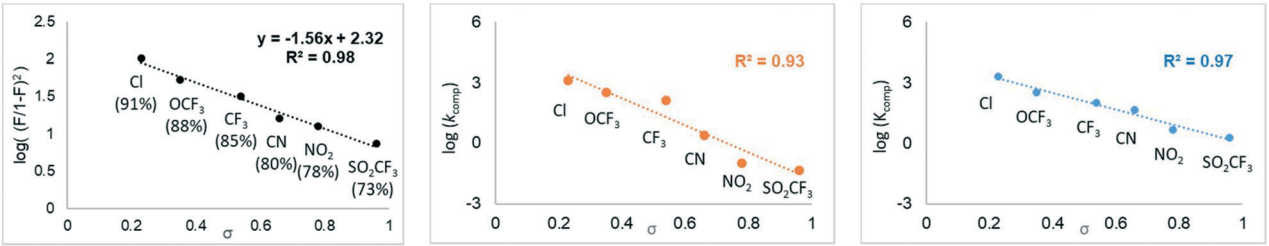

Fig. 2 Left: Experimental Hammett study of 4-substituted anilines, showing correlation between $\log[(F/1-F)^2]$ and σ at 25 °C. Fraction of mixed carbamate (F) in parenthesis. Middle: Computed Hammett plot, showing correlation between σ and the rate constant k (calculated from computed $\Delta G^{\neq}$, 1 atm, Table 3), and right: computed Hammett plot, showing correlation between σ and the equilibrium constant K (calculated from computed ΔG_r, 1 atm, Table 3).

$$F = \frac{[RC_6H_4NHCO_2^-]}{[RC_6H_4NHCO_2^-] + [RC_6H_4NH_2]} \quad (6)$$

$$K = \left(\frac{F}{1-F}\right)^2 \frac{1}{[CO_2]} \quad (7)$$

$$\log\left(\left(\frac{F}{1-F}\right)^2\right) = \sigma\rho + (\log[CO_2] + \log K_0) \quad (8)$$

The ratios of F, obtained by ^{1}H NMR, were plotted against known Hammett constants (σ, Fig. 2, left).[44] As expected, increasing electron density in anilines (σ approaches 0) shifts the equilibrium towards mixed carbamate (larger F). For example, the least electron-deficient aniline (4-Cl) in the series had a 91% conversion to mixed carbamate. The linear plot of eqn (8) gave a good correlation (R^2 = 0.98) using the standard σ values. For four of the substituents, alternative Hammett parameters σ^+ were available,[21] which provided a worse fit (R^2 = 0.94, Fig. S8†). Overall, even highly electron-deficient anilines displayed a high degree of carboxylation, as is seen in the low ρ value (−1.56).

In order to evaluate the reliability of our computational approach, we computed the Hammett plot based on a molecular model composed of TMG, an aromatic amine and CO_2. Gratifyingly, the correlation between the Hammett constants and the computed reaction energies (Table 3) is very good (R^2 = 0.97, Fig. 2, right) and is consistent with the experimental product yields (Fig. 2, left). We note that the computed slope is the same regardless if 1 atm or 1 M standard state energies are employed. The results indicate that the computational model is able to capture the trend of these systems well. However, the computed exergonicity for carboxylation of the less electron-deficient substrates appears somewhat too large (Table 3) compared to experiment (Table 1). Interestingly, the computed barriers for path 2 with the different anilines (Table 3) also provide a relatively good correlation with σ (R^2 = 0.93, Fig. 2, middle).

The combined experimental and computational results indicate that the most likely mechanistic pathway for mixed carbamate formation is the concerted path 2 (Scheme 4), where the role of the superbase is to activate and deprotonate the nucleophile at the carboxylation TS. However, the computations also clearly indicate that a TMG–CO_2 zwitterion is kinetically and thermodynamically accessible. We thus turned towards exploring this species further.

Isolated zwitterion of TMG and CO_2

The existence of zwitterionic CO_2 adducts of superbases has been debated for nearly two decades. Many studies have tried to capture this elusive species, yet only bicarbonate salts have been isolated due to the presence of residual water.[25,30,45] In a major breakthrough, Villiers and co-workers isolated the adduct of CO_2 and TBD, stabilized by an internal hydrogen bond.[19] Since then, CO_2 capture has been observed for cyclic superbases TBD and MTBD in solution, but no reactivity was observed for acylic TMG.[11,24] However, TMG–CO_2 zwitterion **4** has been observed as a minor component in a solid mixture, but its isolation in pure form was not reported.[20]

We reasoned that **4** is transient at room temperature (RT) in solution, as indicated by the computational results (Fig. 1), yet **4** could be more stable at lower temperatures. Low temperature experiments on superbases have been suggested,[25] but to the best of our knowledge, the only successful application has been made with N-heterocyclic imines (NHI),[46] and none with more common superbases, such as TMG or DBU.

We saturated an acetonitrile solution of liquid TMG with CO_2 (1 atm) at RT under strictly anhydrous conditions. The clear solution was stored in a freezer overnight, depositing a white amorphous solid. Filtration of the cold solution using Schlenk technique under CO_2 yielded TMG–CO_2 zwitterion **4**

Table 3 Computed barriers and Gibbs free reaction energies (kcal mol^{-1}, 298 K) for formation of mixed carbamates from 4-substituted anilines[a]

Substituent	Base	$\Delta G^{\neq b}$ 1 atm [1 M]	ΔG_r 1 atm [1 M]
–Cl	TMG	13.2 [11.3]	−4.5 [−6.4]
–OCF_3	TMG	14.0 [12.1]	−3.4 [−5.3]
–CF_3	TMG	14.6 [12.7]	−2.7 [−4.6]
–CN	TMG	16.9 [15.1]	−2.2 [−4.1]
–NO_2	TMG	18.8 [16.9]	−0.8 [−2.7]
–SO_2CF_3	TMG	19.3 [17.4]	−0.3 [−2.2]

[a] PBE0-D3BJ/IEFPCM, see ESI† section 4 for details. Energies are relative to the 4-substituted aniline–TMG pre-associated complex and are given as computed (1 atm) and with a standard state correction to 1 M. [b] For path 2 (Scheme 4).

as a white solid (62% yield). When placed in d_6-DMSO, the solid produced small bubbles of CO_2. Analysis of the solution by NMR showed significant ^{1}H downfield shift of ═NH to 6.58 ppm (freebase 5.34 ppm), and the carbonyl shifted upfield to 165.4 ppm ^{13}C (freebase 166.2 ppm). A long ^{13}C NMR experiment revealed the carboxylate at 126.8 ppm as a broad signal (Fig. 3). Moreover, identical ^{13}C spectra were obtained when the zwitterion was generated *in situ* from TMG under CO_2 (1 atm). Known DBN–CO_2 zwitterion displayed a similar broad carboxylate signal at 136.3 ppm in d_6-DMSO.[46] Note that free CO_2 appears as a sharp signal at 124.2 ppm in d_6-DMSO.[47]

Adduct formation between a Lewis base and a Lewis acid is routinely assessed within frustrated Lewis pair (FLP) chemistry using NMR.[48–51] It is generally accepted that a lack of apparent change in chemical shift (at room temperature) does not exclude adduct formation.[48–51] The absence of any observable change in chemical shift simply indicates any hypothetical adduct equilibrium must lie far to the dissociation side.[48] A reliable way to determine if an equilibrium process is present or not, is to perform a variable-temperature (VT) NMR study.[49–51] In this regard, we studied TMG in d_7-DMF, similar in properties to d_6-DMSO but melting at lower temperatures (Fig. 4). Upon applying CO_2 (1 atm) at 25 °C, the broad carboxylate signal appeared at 125.9 ppm. The ^{1}H signal of ═NH shifted downfield to 5.56 ppm, while the corresponding ^{15}N signal shifted upfield by 1.0 ppm to −207.4 ppm. These changes indicate ═NH is attaining increased sp^3-character through quaternarization, supporting the formation of TMG–CO_2 **4**. The general behavior of ^{1}H and ^{15}N signals of ═NH continued as the temperature was lowered, reaching 5.91 ppm and −209.5 ppm at 0 °C. Likewise, the carboxylate ^{13}C signal was sensitive to temperature, becoming sharper and moving downfield to 128.7 ppm at 0 °C. The thermal behavior of ^{1}H, ^{15}N and ^{13}C signals shows that **4** is stabilized by lower temperatures, thereby being present in larger concentrations. At subzero temperatures, **4** began to precipitate out, and the carboxylate signal was lost. The ^{1}H signal of ═NH continued the previous trend, reaching 6.42 ppm and becoming very broad. In contrast, the ^{15}N signal moved downfield to −205.8 ppm, which likely corresponds to the decreased concentration of **4** in solution. Overall, ^{15}N NMR appears to be highly sensitive for changes at the CO_2-bearing nitrogen (imine-like ═NH), reflecting the subtle changes observed by ^{1}H and ^{13}C NMR. Although we obtained good quality spectra generally in *ca.* 15 h, ^{15}N-labelling of the CO_2-bearing nitrogen could be advantageous if shorter measurements are desired.

To demonstrate the general usefulness of VT and ^{15}N NMR in studying superbase–CO_2 adducts, we investigated formation of DBU–CO_2, which has been debated.[25,30,46] We were able to observe the characteristic broad carboxylate ^{13}C signal at 125.6 ppm in d_7-DMF at 25 °C under CO_2 (1 atm, Fig. S28†). Although changes in ^{1}H and ^{13}C NMR were minimal at 25 °C, ^{15}N NMR revealed a 2.7 ppm upfield shift for the imine-like nitrogen, indicating zwitterion formation. As the temperature was decreased, the carboxylate ^{13}C signal intensified and sharpened, reaching 126.7 ppm at −70 °C, which was accompanied by significant line broadening in ^{1}H NMR. Our results indicate zwitterionic DBU–CO_2 can form, but it is significantly more unstable than TMG–CO_2 or DBN–CO_2. Calculations predict DBU–CO_2 formation to be exergonic at −50 °C and below (ESI† section 4.6). Furthermore, calculations suggest DBN–CO_2 is stabilized by C–H···O interactions between the carboxylate and adjacent methylene groups (ESI† section 4.7), as is observed in the X-ray structure.[46] In contrast, the C–H···O interactions of DBU–CO_2 are weaker, likely due to geometrical restraints of the larger ring size, and not due to sterics as has been proposed.[46] For detailed discussion and spectra, see ESI† section 11.

To our surprise, solid TMG–CO_2 **4** showed no signs of decomposition visually or by NMR when stored under CO_2 at RT for six months. Unfortunately, our attempts to grow X-ray quality crystals of zwitterion **4** were unsuccessful. Therefore, we had to rule out any possibility of the corresponding

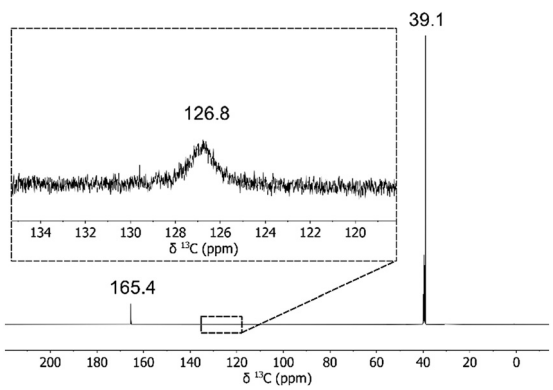

Fig. 3 ^{13}C{^{1}H} NMR spectrum of zwitterion **4**, dissolved in d_6-DMSO in air.

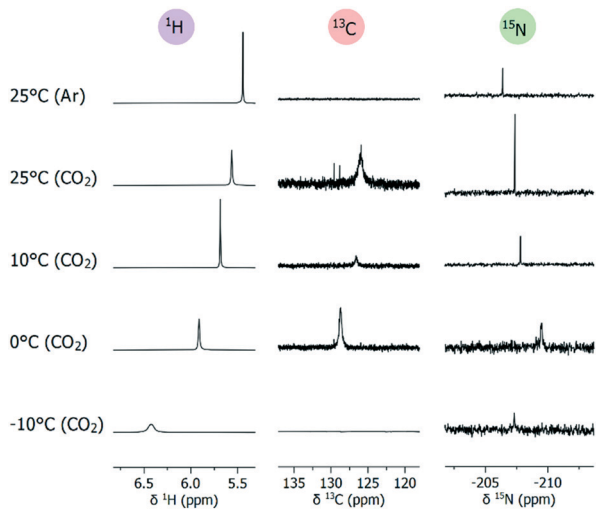

Fig. 4 Variable-temperature NMR spectra (selected regions) of *in situ* generated zwitterion **4** in d_7-DMF. ^{15}N NMR (^{1}H-coupled) obtained at natural abundance. For complete spectra, see ESI† section 9.

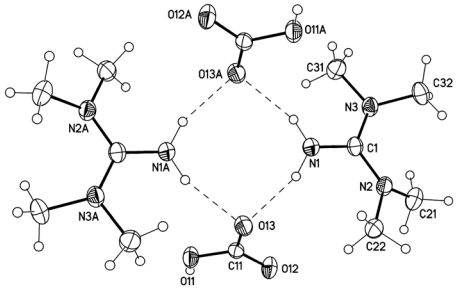

Fig. 5 Structure of the dimer with C_i-symmetry of **5** [TMGH$^+$][HCO$_3^-$] (symmetry operator $-x + 1, -y + 1, -z + 1$, displacement parameters are drawn at 50% probability level).

hydrolysis product, bicarbonate **5** [TMGH$^+$][HCO$_3^-$]. We decided to independently synthesize **5**, and perform a comparative characterization with **4**. Repeating the synthesis in the presence of water (1 equiv. to TMG) resulted in the immediate precipitation of **5** at RT. We were able to characterize bicarbonate **5** by NMR (HCO_3^- at 158.3 ppm) and X-ray (Fig. 5).[52]

We assessed the thermal stability of zwitterion **4** and bicarbonate **5** by thermogravimetric and differential thermal analysis under a flow of dry N_2 (Fig. 6). At 25 °C, zwitterion **4** slowly degraded under the N_2-flow, consistent with previous reports of CO_2-adduct lability.[12] The onset of thermal degradation (CO_2 release) began at 44 °C, reaching a maximum at 51 °C. The major peak at 153 °C corresponds to evaporation of TMG (bp. 160 °C).[53] In contrast, bicarbonate **5** showed significantly improved thermal stability. Onset of degradation occurred at 80 °C, and reaching maxima at 103 °C and 112 °C, corresponding to decomposition of the bicarbonate ion.

The IR spectra of zwitterion **4** and bicarbonate **5** was compared to known compounds (Table 4). The asymmetric CO_2 stretching band in zwitterion **4** (entry 1) is similar in value to reported CO_2 adducts of N-heterocyclic carbene (NHC, entry 3)[54] and NHI (entry 4).[46] Bicyclic superbase–CO_2 zwitterions appear at higher frequencies (entries 5 and 6), suggesting the steric strain of the carboxylate in zwitterion **4** is similar to NHC and NHI.[54] In contrast, bicarbonate **5** has a significantly lowered frequency (entry 2). The IR spectra of zwitterion **4** and bicarbonate **5** show significant differences (Fig. S50 and S51†). For example, zwitterion **4** shows relatively strong and sharp peaks at 3035 and 3019 cm^{-1}, indicative of polymeric or dimeric association.[55] In contrast, bicarbonate **5** has low to medium intensity broad bands in the regions of 2600–3100 cm^{-1}, indicative of dimeric –OH···O=C interaction,[55] as is seen in the X-ray structure (Fig. 5).

When decarboxylation temperatures are compared, it is observed that zwitterion **4** falls in line with other Lewis base–CO_2 adducts, with the exception of significantly more stable NHC–CO_2 (Table 4, entry 3). As seen in Table 4, zwitterion **4** displays physical attributes very similar to known Lewis base–CO_2 adducts, while bicarbonate **5** deviates from most CO_2-adducts by being thermally more robust.

We further investigated the identity of **4** and **5** by performing computational studies on the monomers and dimers of both species (Fig. 7). It can be noted that dimeric **4** with our computational protocol is several kcal mol^{-1} more stable than the separated monomers, possibly due to hydrogen bonding (ΔG_r = −3.1 kcal mol^{-1} [1 atm], −4.9 kcal mol^{-1} [1 M]). Further, the computed asymmetric CO_2 stretching band of dimeric **4** is 1659 cm^{-1} (Fig. 7), in excellent agreement with the experimental frequency of 1661 cm^{-1} (Table 4). The monomeric **4** has a significantly higher computed frequency (1690 cm^{-1}), whereas the monomer and dimer of **5** both have lower frequencies, in agreement with experiment (Table 4).

The combined results confirm the identity of zwitterion **4** and bicarbonate **5**. Given the transient existence of superbase–CO_2 adducts in solution at RT, why is zwitterion **4** isolable from a cold solution? Here, it is probable TMG is rapidly carboxylated, yet the resulting zwitterion decomposes rapidly at 298 K, in agreement with the computed energies (Scheme 5), showing a low barrier for formation of **4** (8.7 kcal mol^{-1}), but a slightly endergonic reaction (0.4 kcal mol^{-1}). At lower temperatures, the entropic penalty is reduced and solvent induced dissociation of **4** into TMG and CO_2 is slower

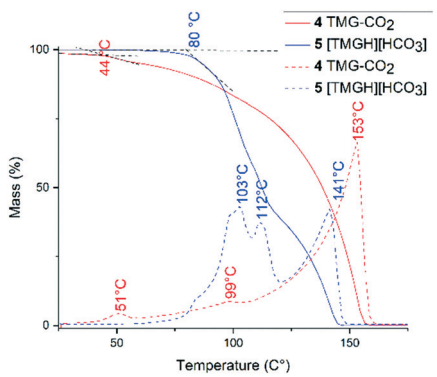

Fig. 6 Thermogravimetric (full line) and differential thermal analysis (dashed line) of zwitterion **4** and bicarbonate **5**. Intersection of black dashed lines indicates onset of thermal degradation.

Table 4 Frequency of the asymmetric CO_2 stretching band and decarboxylation temperatures (T) of Lewis base–CO_2 adducts

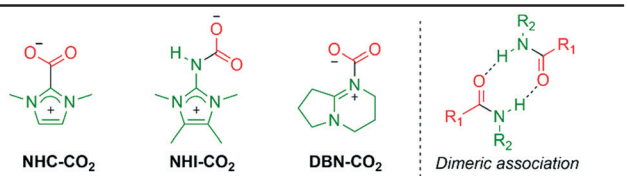

Entry	Adduct	IR (cm^{-1})	T (°C)	Ref.
1	**4** TMG–CO_2	1661	44	This work
2	**5** [TMGH$^+$][HCO$_3^-$]	1600	80	This work
3	NHC–CO_2	1653	162	Ref. 54
4	NHI–CO_2	1662	35	Ref. 46
5	TBD–CO_2	1712	40	Ref. 19
6	DBN–CO_2	1727	30	Ref. 46

1,5-Diazabicyclo[4.3.0]non-5-ene = DBN.

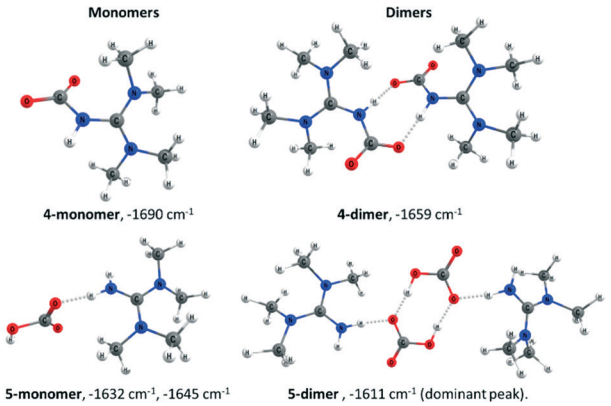

Fig. 7 Computed structures and asymmetric CO_2 stretching band of the monomer and dimer of **4** and **5**. For **5**-monomer, two equally strong peaks are observed and for **5**-dimer, some CO_2 asymmetric stretching contribution is also observed for a peak at 1652 cm^{-1}, besides the dominant peak at 1611 cm^{-1}.

(see NMR discussion, *vide supra*). Indeed, calculations indicate that formation of **4** from CO_2 and TMG would be slightly exergonic at 263 K (−0.7 kcal mol^{-1}, Scheme 5). At subzero temperatures, the higher concentration of **4** leads to aggregates, which precipitate out. According to calculations, formation of dimer **4′** is exergonic (Fig. S5†).

Having established **4** as a true zwitterion, we set out to explore its reactivity under neat conditions, in order to eliminate solvent induced dissociation of CO_2. In a glovebox, we added liquid protic nucleophiles **6a–c** to solid zwitterion **4**, resulting in an immediate reaction of bubbling (CO_2) and gel formation (slowly solidifying). Analysis by NMR showed successful carboxylation of aromatic amine **7a**, pyrrole **7b**, and 1-butanol **7c** (Scheme 6), although **7a** was obtained in somewhat lower yield compared to the *in situ* experiment (Fig. 2, left). These experiments support that CO_2 dissociates from zwitterion **4** before carboxylation occurs, in accord with the calculations (Fig. 1). Similar stoichiometric carboxylations have been performed with TBD–CO_2 in solution, but the necessity of CO_2 dissociation from TBD–CO_2 was not discussed.[56]

Lewis base–CO_2 adducts have been reported to carboxylate amines,[20,30] however, their chemical identity has been debated, as others have suggested the adducts are better described as bicarbonate salts.[25] Therefore, we repeated our

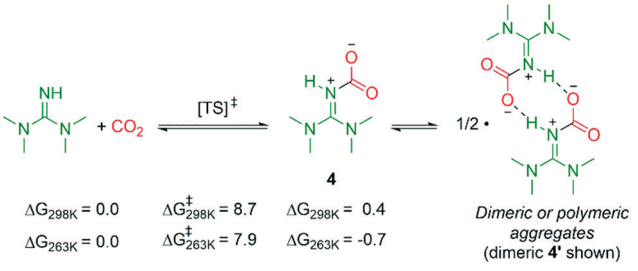

Scheme 5 Computed free energies (kcal mol^{-1}, PBE0-D3BJ/IEFPCM[acetonitrile], 1 M standard state) for reversible formation of zwitterion **4**.

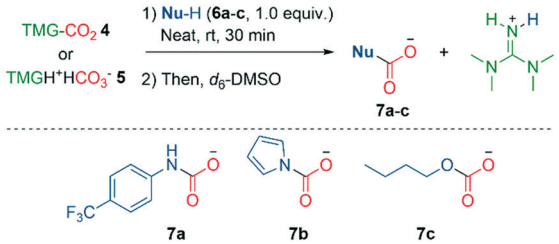

	7a	7b	7c
Using **4**	47%	56%	26%
Using **5**	33%	36%	24%

Scheme 6 Carboxylation of protic nucleophiles using solid zwitterion **4** or bicarbonate **5** on 0.5 mmol scale. Yields determined by ^{1}H NMR.

experiments in Scheme 6 with bicarbonate **5**. No bubbles were observed, although the mixtures did solidify. Carboxylation of 1-butanol **7c** was similar in yield, while bicarbonate **5** was significantly less effective at carboxylating nitrogen compounds. We recommend future superbase–CO_2 zwitterion studies to include the corresponding bicarbonate as a control in carboxylation reactions. Tetraalkylammonium bicarbonate salts are able to carboxylate amines,[57] but not pyrroles.[58] Considering **5** readily carboxylated pyrrole **7b**, this suggests the presence of TMG is critical.

In summary, zwitterionic TMG–CO_2 **4** may exist under the carboxylation conditions, in agreement with the low barrier computed for its formation (Fig. 1), however, our mechanistic analysis indicates that **4** is likely to dissociate into TMG and CO_2 prior to carboxylation (see mechanistic discussion, *vide supra*). At low temperatures, dissociation is slowed down, allowing isolation of **4**. We further note that the experiments in Scheme 6 showcase the potential of zwitterion **4** as a source of dry CO_2,[46] and that carboxylations are possible without an atmosphere (large excess) of CO_2.

Conclusions

Previous literature has proposed zwitterionic superbase–CO_2 adducts as active carboxylation agents. In this work, we were able to isolate pure TMG–CO_2 as a stable solid, allowing us to explore its carboxylation reactivity. Our experimental and computational results indicate that CO_2 must first dissociate from the TMG–CO_2 zwitterion before carboxylation can occur. This opens a low energy pathway, where the base pre-associates to the nucleophile, activating it towards attack at a free CO_2, with carboxylation and deprotonation occurring concertedly (path 2, Scheme 4).

The identity of the TMG–CO_2 zwitterion was confirmed by NMR and computational studies, in addition to a comparative analysis of the corresponding hydrolysis product (bicarbonate). Room temperature NMR studies were used to observe TMG–CO_2 and the long-sought DBU–CO_2 adduct, both displaying a broad carboxylate ^{13}C signal, due to reversible binding of CO_2. These results were complimented by VT NMR studies. Natural abundance ^{15}N NMR was found to be sensitive for zwitterion formation, with significant

upfield shifts of the CO_2-bearing nitrogen, which was introduced here as a highly useful tool for studying superbase interactions with CO_2.

Our experimental and computational findings are significant for further design and development of CO_2-based synthesis, because they demonstrate that superbases are able to activate dormant species, such as aromatic amines, which are otherwise inert towards CO_2. For example, as shown in this work, both zwitterionic TMG–CO_2 and the corresponding bicarbonate can carboxylate nucleophiles without an atmosphere of CO_2 (large excess). However, zwitterionic TMG–CO_2 was significantly more effective at carboxylating nitrogen nucleophiles. Although the carboxylation is stoichiometric in superbase, we foresee increasing use of superbases as activating agents in many catalytic applications. In this context, a very important observation is that although superbases can transiently bind and store CO_2, the resulting zwitterion is not a form of "activated CO_2".

Author contributions

JKM conceived the project. JKM, TT, and AS carried out the experiments. LP and KHH performed the computational studies. MN performed the X-ray crystallography studies. The manuscript and supplemental information was prepared jointly by all authors. TR supervised the experimental work, and KHH the computational work.

Conflicts of interest

There are no conflicts to declare.

Acknowledgements

We thank Dr. Lauri Partanen for his advice regarding equilibrium studies, Dr. Kristina Sorochkina for her insightful comments, and Dr. David Casadio and Dr. Sami Heikkinen for their help with NMR studies. This work has been supported by CHEMS – The Doctoral Programme in Chemistry and Molecular Sciences at University of Helsinki, Academy of Finland (project 310767), NordForsk (Grant No. 85378) and the members of the Nordic Consortium for CO_2 Conversion (NordCO_2), and Nylands Nation (JKM). KHH thanks the Tromsø Research Foundation (TFS2016KHH), the Research Council of Norway (grant No. 300769 and 262695) and Sigma2 for grants of computer time (No. nn9330k and nn4654k).

Notes and references

1 A. Hager, N. Vrielink, D. Hager, J. Lefranc and D. Trauner, *Nat. Prod. Rep.*, 2016, **33**, 491–522.
2 A. Ricci, *Modern amination methods*, John Wiley & Sons, Inc., 2007.
3 E. Vitaku, D. T. Smith and J. T. Njardarson, *J. Med. Chem.*, 2014, **57**, 10257–10274.
4 B. Dutcher, M. Fan and A. G. Russell, *ACS Appl. Mater. Interfaces*, 2015, **7**, 2137–2148.
5 T. Niemi and T. Repo, *Eur. J. Org. Chem.*, 2018, 1180–1188.
6 J. Vaitla, Y. Guttormsen, J. K. Mannisto, A. Nova, T. Repo, A. Bayer and K. H. Hopmann, *ACS Catal.*, 2017, **7**, 7231–7244.
7 F. D. Bobbink, S. Das and P. J. Dyson, *Nat. Protoc.*, 2017, **12**, 417–428.
8 J. K. Mannisto, A. Sahari, K. Lagerblom, T. Niemi, M. Nieger, G. Sztanó and T. Repo, *Chem. – Eur. J.*, 2019, **25**, 10284–10289.
9 W. Schilling and S. Das, *ChemSusChem*, 2020, **13**, 6246–6258.
10 D. Riemer, P. Hirapara and S. Das, *ChemSusChem*, 2016, **3**, 1916–1920.
11 P. V. Kortunov, M. Siskin, L. S. Baugh and D. C. Calabro, *Energy Fuels*, 2015, **29**, 5940–5966.
12 P. V. Kortunov, L. S. Baugh, M. Siskin and D. C. Calabro, *Energy Fuels*, 2015, **29**, 5967–5989.
13 C. Chiappe, G. Pampaloni, L. Biancalana, G. Bresciani and F. Marchetti, *New J. Chem.*, 2017, **41**, 1798–1805.
14 W. McGhee, D. Riley, K. Christ, Y. Pan and B. Parnas, *J. Org. Chem.*, 1995, **60**, 2820–2830.
15 A. L. Ethier, J. R. Switzer, A. C. Rumple, W. Medina-Ramos, Z. Li, J. Fisk, B. Holden, L. Gelbaum, P. Pollet, C. A. Eckert and C. L. Liotta, *Processes*, 2015, **3**, 497–513.
16 W. D. McGhee, D. P. Riley, M. E. Christ and K. M. Christ, *Organometallics*, 1993, **12**, 1429–1433.
17 M. Costa, G. P. Chiusoli and M. Rizzardi, *Chem. Commun.*, 1996, 1699–1700.
18 K. Masuda, Y. Ito, M. Horiguchi and H. Fujita, *Tetrahedron*, 2005, **61**, 213–229.
19 C. Villiers, J. P. Dognon, R. Pollet, P. Thuéry and M. Ephritikhine, *Angew. Chem., Int. Ed.*, 2010, **49**, 3465–3468.
20 F. S. Pereira, E. R. de Azevedo, E. F. da Silva, T. J. Bonagamba, D. L. da Silva Agostíni, A. Magalhães, A. E. Job and E. R. Pérez González, *Tetrahedron*, 2008, **64**, 10097–10106.
21 Z. Xin, C. Lescot, S. D. Friis, K. Daasbjerg and T. Skrydstrup, *Angew. Chem., Int. Ed.*, 2015, **54**, 6862–6866.
22 H. C. Fu, F. You, H. R. Li and L. N. He, *Front. Chem.*, 2019, **7**, 1–15.
23 H. Zhou, W. Chen, J. H. Liu, W. Z. Zhang and X. B. Lu, *Green Chem.*, 2020, **22**, 7832–7838.
24 R. Nicholls, S. Kaufhold and B. N. Nguyen, *Catal. Sci. Technol.*, 2014, **4**, 3458–3462.
25 D. J. Heldebrant, P. G. Jessop, C. A. Thomas, C. A. Eckert and C. L. Liotta, *J. Org. Chem.*, 2005, **70**, 5335–5338.
26 W. Li, N. Yang and Y. Lyu, *Org. Chem. Front.*, 2016, **3**, 823–835.
27 M. Hulla and P. J. Dyson, *Angew. Chem.*, 2020, **59**, 1002–1017.
28 M. Hulla, S. M. A. Chamam, G. Laurenczy, S. Das and P. J. Dyson, *Angew. Chem., Int. Ed.*, 2017, **56**, 10559–10563.
29 P. V. Kortunov, M. Siskin, M. Paccagnini and H. Thomann, *Energy Fuels*, 2016, **30**, 1223–1236.
30 E. R. Pérez, R. H. A. Santos, M. T. P. Gambardella, L. G. M. De Macedo, U. P. Rodrigues-Filho, J. C. Launay and D. W. Franco, *J. Org. Chem.*, 2004, **69**, 8005–8011.

31 M. J. Diem, D. F. Burow and J. L. Fry, *J. Org. Chem.*, 1977, **42**, 1801–1802.
32 J. E. Rainbolt, P. K. Koech, C. R. Yonker, F. Zheng, D. Main, M. L. Weaver, J. C. Linehan and D. J. Heldebrant, *Energy Environ. Sci.*, 2011, **4**, 480–484.
33 N. von Wolff, C. Villiers, P. Thuéry, G. Lefèvre, M. Ephritikhine and T. Cantat, *Eur. J. Org. Chem.*, 2017, **2017**, 676–686.
34 M. Baidya and H. Mayr, *Chem. Commun.*, 2008, 1792–1794.
35 A. Gholamipour-Shirazi and C. Rolando, *Org. Biomol. Chem.*, 2012, **10**, 8059–8063.
36 V. A. Bren', E. N. Maloesheva and V. I. Minkin, *Org. React.*, 1967, **4**, 534–555.
37 E. I. Rõõm, A. Kütt, I. Kaljurand, I. Koppel, I. Leito, I. A. Koppel, M. Mishima, K. Goto and Y. Miyahara, *Chem. – Eur. J.*, 2007, **13**, 7631–7643.
38 D. J. Heldebrant, P. K. Koech, J. E. Rainbolt, F. Zheng, T. Smurthwaite, C. J. Freeman, M. Oss and I. Leito, *Chem. Eng. J.*, 2011, **171**, 794–800.
39 I. Kaljurand, A. Kütt, L. Sooväli, T. Rodima, V. Mäemets, I. Leito and I. A. Koppel, *J. Org. Chem.*, 2005, **70**, 1019–1028.
40 K. Kaupmees, A. Trummal and I. Leito, *Croat. Chem. Acta*, 2014, **87**, 385–395.
41 C. M. Zall, J. C. Linehan and A. M. Appel, *ACS Catal.*, 2015, **5**, 5301–5305.
42 Substituents with Hammett constants below a certain threshold ($\sigma \leq 0$) would all produce the same result (100% yield), prohibiting us from constructing a linear correlation.
43 L. P. Hammett, *J. Am. Chem. Soc.*, 1937, **59**, 96–103.
44 C. Hansch, A. Leo and R. W. Taft, *Chem. Rev.*, 1991, **91**, 165–195.
45 I. Tiritiris, J. Mezger, E. V. Stoyanov and W. Kantlehner, *Z. Naturforsch., B: J. Chem. Sci.*, 2011, **66**, 407–418.
46 L. F. B. Wilm, T. Eder, C. Mück-Lichtenfeld, P. Mehlmann, M. Wünsche, F. Buß and F. Dielmann, *Green Chem.*, 2019, **21**, 640–648.
47 G. R. Fulmer, A. J. M. Miller, N. H. Sherden, H. E. Gottlieb, A. Nudelman, B. M. Stoltz, J. E. Bercaw and K. I. Goldberg, *Organometallics*, 2010, **29**, 2176–2179.
48 S. Tanaka, Y. Saito, T. Yamamoto and T. Hattori, *Org. Lett.*, 2018, **20**, 1828–1831.
49 A. Y. Houghton, J. Hurmalainen, A. Mansikkamäki, W. E. Piers and H. M. Tuononen, *Nat. Chem.*, 2014, **6**, 1–6.
50 A. C. Shaikh, J. M. Veleta, J. Moutet and T. L. Gianetti, *Chem. Sci.*, 2021, **12**, 4841–4849.
51 L. Greb, P. Oña-Burgos, B. Schirmer, S. Grimme, D. W. Stephan and J. Paradies, *Angew. Chem., Int. Ed.*, 2012, **51**, 10164–10168.
52 X-Ray Data for **5** (CIF), CCDC 2044161, contains the Supplementary Crystallographic Data for this paper. It is a redetermination of COWGON at 123 K using Cu-Kα radiation. Refcode COWGON: CCDC-1912766; V. Ramkumar and R. L. Gardas, *J. Chem. Eng. Data*, 2019, **64**, 4844–4855; A related hemihydrate has been reported. Refcode IQAPIA, CCDC-796566. See ref. 45.
53 A. E. Sherr and A. A. Krupnik, *J. Appl. Polym. Sci.*, 1965, **9**, 2707–2714.
54 B. R. Van Ausdall, J. L. Glass, K. M. Wiggins, A. M. Aarif and J. Louie, *J. Org. Chem.*, 2009, **74**, 7935–7942.
55 T. Hase, *Tables for Organic Spectrometry*, Otatieto, 10th edn, 2008.
56 C. D. N. Gomes, O. Jacquet, C. Villiers, P. Thuéry, M. Ephritikhine and T. Cantat, *Angew. Chem., Int. Ed.*, 2012, **51**, 187–190.
57 A. Inesi, V. Mucciante and L. Rossi, *J. Org. Chem.*, 1998, **3263**, 1337–1338.
58 S. Cesa, V. Mucciante and L. Rossi, *Tetrahedron*, 1999, **55**, 193–200.